PHOTONICS Research

Theoretical aspects and sensing demonstrations of cone-shaped inwall capillary-based microsphere resonators

Xiaobei Zhang,[1,*] Yong Yang,[1] Huawen Bai,[1] Jiawei Wang,[1] Ming Yan,[1] Hai Xiao,[2] and Tingyun Wang[1]

[1]Laboratory of Specialty Fiber Optics and Optical Access Networks, Shanghai Institute for Advanced Communication and Data Science, School of Communication and Information Engineering, Shanghai University, Shanghai 200072, China
[2]Department of Electrical and Computer Engineering, Clemson University, Clemson, South Carolina 29634, USA
*Corresponding author: xbzhang@shu.edu.cn

Received 25 July 2017; revised 27 August 2017; accepted 27 August 2017; posted 30 August 2017 (Doc. ID 303294); published 28 September 2017

In this paper, a detailed theoretical study on the characteristics of cone-shaped inwall capillary-based microsphere resonators is described and demonstrated for sensing applications. The maximum, minimum, slope, contrast, and width of the Fano resonance are analyzed. As the transmission coefficient of the capillary resonator increases, the absolute value of the slope of Fano resonances increases to reach its maximum, which is useful for sensors with an ultra-high sensitivity. There occurs another phenomenon of electromagnetically induced transparency when the reflectivity at the capillary–environment interface is close to 100%. We also experimentally demonstrated its capability for temperature and refractive index sensing, with a sensitivity of 10.9 pm/°C and 431 dB/RIU based on the Fano resonance and the Lorentzian line shape, respectively.

OCIS codes: (230.5750) Resonators; (060.2370) Fiber optics sensors.

https://doi.org/10.1364/PRJ.5.000516

1. INTRODUCTION

The underlying physics of whispering gallery modes (WGMs) is that the electromagnetic waves are trapped by the continuous inner total reflection and circle along the wall of the microcavity [1]. Because of the extremely high Q-factors and small mode volume of the WGMs, WGM microcavities have been widely investigated and demonstrated for various applications [2–8]. The typical spectrum of WGM microcavities is the symmetric Lorentzian line shape. Under special configurations, the Lorentzian shaped resonances can transform into asymmetric Fano-like resonances, which generally have large slopes for sensing and switching applications. In 2002, Fan designed a structure in which an optical microresonator was side-coupled to a Fabry–Perot cavity embedded in a waveguide, and asymmetric Fano-like resonance line shapes in the transmission spectra were observed [9]. From then on, asymmetric Fano-like resonance line shapes have been observed in a wide variety of configurations of WGM microcavities, such as a WGM microcavity coupled with a Fabry–Perot cavity [9,10], two directly coupled WGM microcavities [11,12], two indirectly coupled WGM microcavities [13–15], a WGM microresonator in an aqueous environment [16], a WGM microcavity coupled with a grating [17], a two-mode polymer coated microcavity [18], and a deformed microcavity [19].

Recently, we proposed a novel and simple cone-shaped inwall capillary-based microsphere resonator to produce Fano resonances [20]. The structure is composed of a single-mode fiber (SMF), a barium titanite glass microsphere, and a capillary with the end face as a reflector. The light reflected from the reflector transforms the symmetric Lorentzian line shapes into Fano resonances. Generally, there are two reflectors in the Fano-resonance-based structures of WGM microcavities, such as those in Refs. [9,10], resulting in an envelope of a Fabry–Perot cavity in the spectrum, which does not exist in our structure. After a long and sharp cone-shaped inwall is obtained by chemical etching, an extremely high coupling efficiency between the optical fiber and capillary can be produced. Moreover, the proposed structure is alignment-free, mechanically robust, and operates in a reflection mode, making it very attractive in many applications. Our previous work has focused on the proof-of-concept of this structure. In this paper, we systematically investigate the characteristics of the structure by simulation and experiment, including analyzing the effects of various factors on Fano resonances by simulation, and experimentally demonstrating the characteristics for temperature and refractive index sensing.

2. THEORETICAL ANALYSES

Figure 1(a) shows the cone-shaped inwall capillary based microsphere resonator, of which the structure, model, and fabrication have been described in Ref. [20], with the normalized reflection P_R given by

$$P_R = \left| r\left(\frac{t - \tau t p^2}{1 - \tau t^2 p^2}\right)^2 \exp(2i\delta) - \frac{\sqrt{\tau}k^2 p}{1 - \tau t^2 p^2}\right|^2, \quad (1)$$

where t and k are the transmission coefficient and coupling coefficient, respectively, of the capillary resonator satisfying the equation $k^2 + t^2 = 1$, under the condition of lossless coupling. τ is the round-trip resonator transmission coefficient. p is halfway phase factor satisfying $p = \exp(i\theta/2)$. θ is the normalized frequency satisfying $\theta = 4\pi^2 n_{\text{eff}} R/\lambda$. n_{eff} is the effective index of the microsphere. R is the radius of the microsphere. λ is the optical wavelength in vacuum. δ and L are the phase difference and distance from the capillary resonator coupling region to the front end face of the capillary, respectively, with $\delta = \beta L$, where β as the propagation constant. r is the reflectivity at the capillary–environment interface satisfying $r = (n_{\text{cap}} - n_{\text{env}})/(n_{\text{cap}} + n_{\text{env}})$, with n_{cap} and n_{env} as the refractive indices of capillary and environment (air, solution, or other coated materials), respectively. Figure 1(b) shows a typical Fano resonance with the definitions of relevant parameters. The width of the Fano resonance $\Delta\theta$ is the difference of the abscissa values of the maximum and minimum. The contrast of the Fano resonance is the difference of the ordinate values of the maximum and minimum, while the slope of the Fano resonance is the slope of the midpoint between the maximum and minimum.

To illustrate the evolution of Fano resonances as functions of the phase difference δ, we set t, τ, and r as 0.95, 0.95, and 20%, respectively. From Eq. (1), we can see that the spectrum is periodic within a period of π and asymmetrical in a period, as shown in Fig. 2(a). The progresses of P_R as a function of the phase difference in four different quadrants ($\pi/4$ each) are plotted in Figs. 2(b)–2(e). Although the resonance depth varies, the maxima and minima occur at about the same locations. This suggests that the phase difference affects mainly the shapes of the spectra, including the traditional Lorentzian line shape and Fano resonances, which can be controlled through the length from the capillary end face to the coupling point.

To study the coupling between the capillary and resonator and its impact on the resonator system, we set the phase difference δ and the reflectivity at the capillary–air interface r as 0.3π and 20%, respectively, and the round-trip resonator transmission coefficient τ to be 0.9, 0.95, and 0.99. We choose the transmission coefficient of the capillary resonator t to vary from 0.880 to 1.0 to investigate the characteristics of the Fano resonances, noting that there is no resonator, and $P_R = |r|^2$ when t equals 1. From Figs. 3(a)–3(c), we find that the maximum becomes smaller and its location does not change regardless

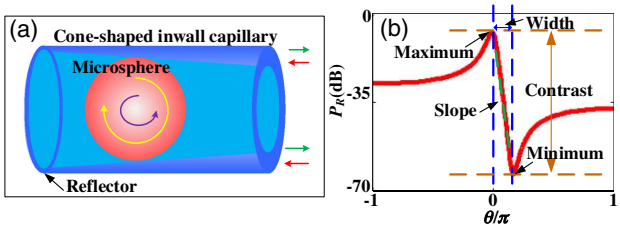

Fig. 1. (a) Schematic of the cone-shaped inwall capillary-based microsphere resonator. (b) A typical Fano resonance and relevant parameter definitions.

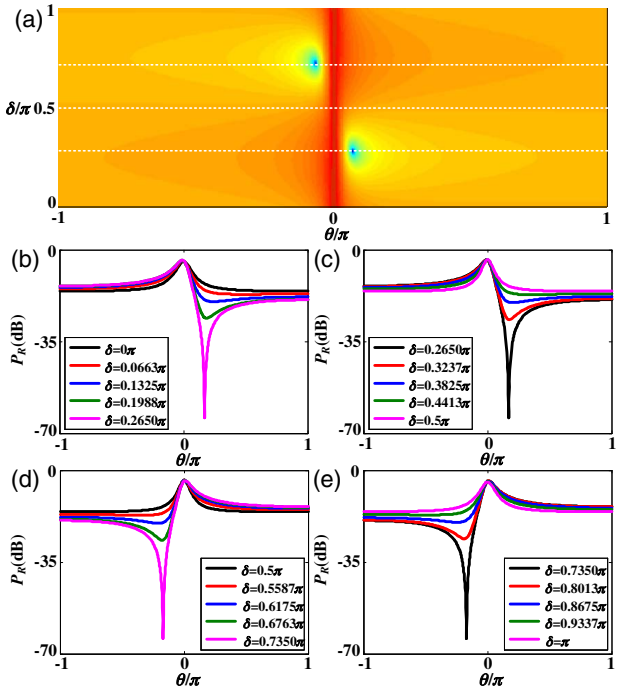

Fig. 2. (a) Simulation of Fano resonances versus normalized frequency and δ (the reflection is normalized). (b)–(e) are the progression of P_R as a function of δ in four quadrants of $\pi/4$ each.

of the value of τ. Meanwhile, the slope changed nonlinearly, as shown in Fig. 3(d). For example, the absolute value of the slope reaches its maximum at about $t = 0.98$ for $\tau = 0.9$. This suggests that the slope can be optimized according to the relation between the resonator loss and the coupling, similar to the critical coupling for the maximal contrast in a traditional taper coupled resonator system.

Figure 3 also indicates that the maximum and minimum values of the Fano resonance change at different conditions. The detailed changing processes are shown in Fig. 4. In Fig. 4(a), the maximum values decrease versus the transmission coefficient t at all values of τ. Moreover, the intensity decreases,

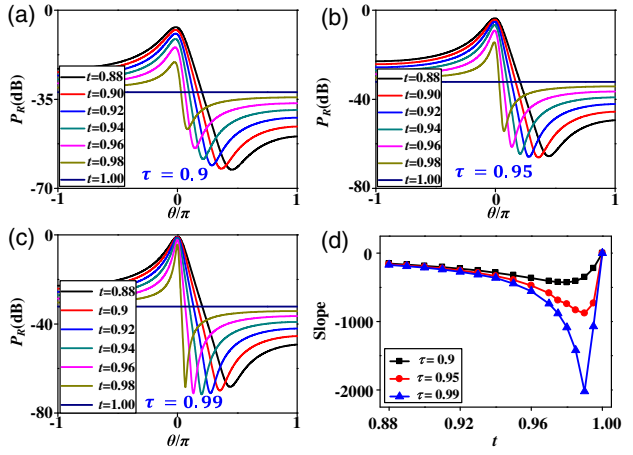

Fig. 3. (a)–(c) Simulations when τ are 0.9, 0.95, and 0.99, respectively. (d) Illustration of the changing process of slope.

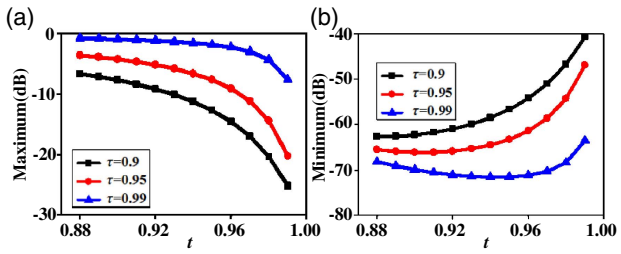

Fig. 4. Simulation of (a) the maximum and (b) the minimum versus t, when τ is 0.9, 0.95, and 0.99.

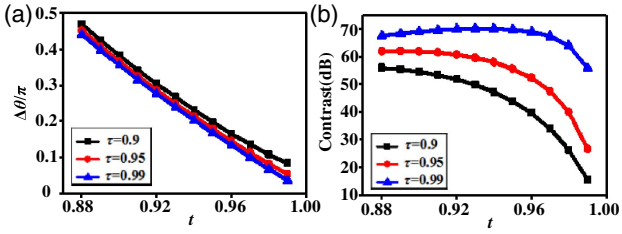

Fig. 5. When τ is 0.9, 0.95, and 0.99, simulation of (a) $\Delta\theta/\pi$ and (b) contrast (dB).

with τ decreasing as a result of the increasing loss of the resonator. In contrast, the minimum values generally increase versus t regardless of the value of τ, as shown in Fig. 4(b), while the intensity increases when τ decreases.

As t increases from 0.880 to 0.999, the width of Fano resonance $\Delta\theta$ decreases nearly linearly regardless of the value of τ. Moreover, the intensity decreases as τ increases, as shown in Fig. 5(a). This is similar to the mode splitting in the system of multiple resonators [21], due to the interactions of light trapped in the resonator and reflected from the capillary front end face. Similarly, the contrast generally also decreases as t increases from 0.880 to 0.999, but not linearly, regardless of the value of τ except for $\tau = 0.99$, as shown in Fig. 5(b). On the contrary, the intensity of the contrast increases due to the decreasing of the resonator loss.

The reflectivity at the capillary–environment interface r can be tailored by coating specific materials. To investigate the effect of r, we first set both τ and t to be 0.95 and choose δ as three typical values: 0, 0.5π, and 0.265π. If the capillary end is immersed into the index matching oil, the reflectivity r equals to 0. When δ equals to 0 and 0.5π, respectively, the resonances in these two cases at first are both Lorentzian shaped, and the contrast of them decreases as r increases from 0 to 100%. When r is close to 100% and the capillary end face is coated with high reflectivity materials such as Au/Ag, the former is a Lorentzian line shape; however, the latter becomes an Lorentzian line shape with a peak inside the dip, as shown in Figs. 6(a) and 6(b). The latter is similar to the previously reported phenomenon named electromagnetically induced transparency (EIT) [11]. When δ is equal to 0.265π, the resonance is always Fano-resonance shaped, and the absolute value of its slope increases. Meanwhile, the width of Fano resonances first decreases and then increases, as shown in Figs. 6(c) and 6(d),

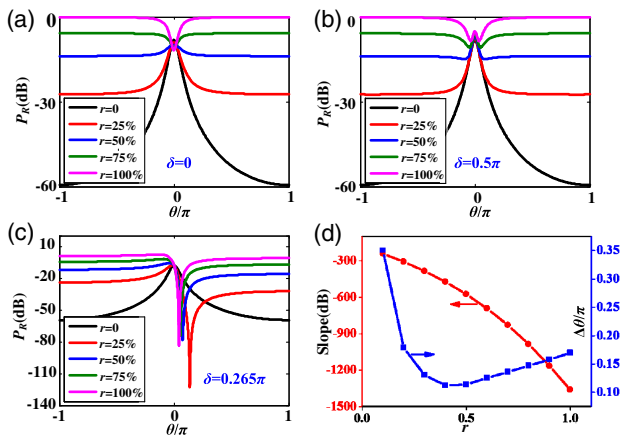

Fig. 6. (a)–(c) Simulations when δ adopted as 0, 0.5π, and 0.265π, respectively, with r increasing from 0 to 100%. (d) The slope and width of the Fano resonances with r increasing from 10% to 100%.

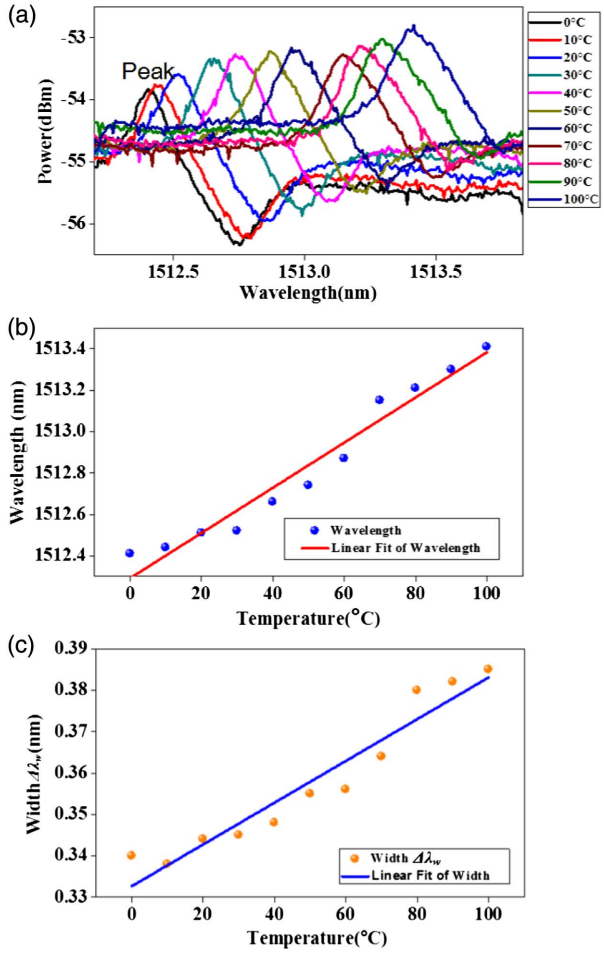

Fig. 7. (a) Spectra, (b) peak wavelength shifts, and (c) width of a Fano resonance when temperature increases.

as r increases from 0 to 100%. Therefore, both the slope and the Fano resonance width can be tailored by the coating method.

3. SENSING DEMONSTRATIONS

The capillary with an inner diameter of 5 μm spliced to the SMF is immersed into hydrofluoric solution, until the thickness of the capillary end wall is etched to 5 μm [20]. Then a microsphere with a diameter of 45 μm and refractive index of 1.93 is inserted into the cone via the precision fiber alignment stage and fiber taper, which is held firmly by the capillary with friction. The microsphere resonator is made of barium titanite glass [20], which is inherently sensitive to temperature and the surrounding environment. As a result, the device can be directly used as a temperature and refractive index sensor. We placed the device into the temperature cabinet and increased temperature from 0°C to 100°C with an interval of 10°C. As the temperature increased, the Fano resonance showed a redshift with a sensitivity of 10.9 pm/°C, as shown in Figs. 7(a) and 7(b). Meanwhile, the width of the Fano resonance $\Delta\lambda_w$ (in the unit of nanometer) became larger, as shown in Fig. 7(c). This is due to the coupling between the resonator and the capillary increases, because the temperature increase will induce the microsphere to become slightly larger. This is also validated by the simulation results in Fig. 5(a), with smaller t corresponding to a larger coupling. According to the temperature sensing principle, there occurs the following relationship between the wavelength shift $\Delta\lambda_0$ at the wavelength λ_0 and the temperature variation ΔT [22]:

$$\frac{\Delta\lambda_0}{\Delta T} = (\alpha + \xi)\lambda_0, \tag{2}$$

where α and ξ are the thermo-expansion coefficient and the thermo-optic coefficient, respectively. As the thermal-expansion coefficient generally is of the order of 10 times the thermo-optic coefficient for the glass, the thermal-expansion effect would be dominant. The theoretical temperature sensitivity is calculated to be 10.85 pm/°C, which agrees with the experimental result.

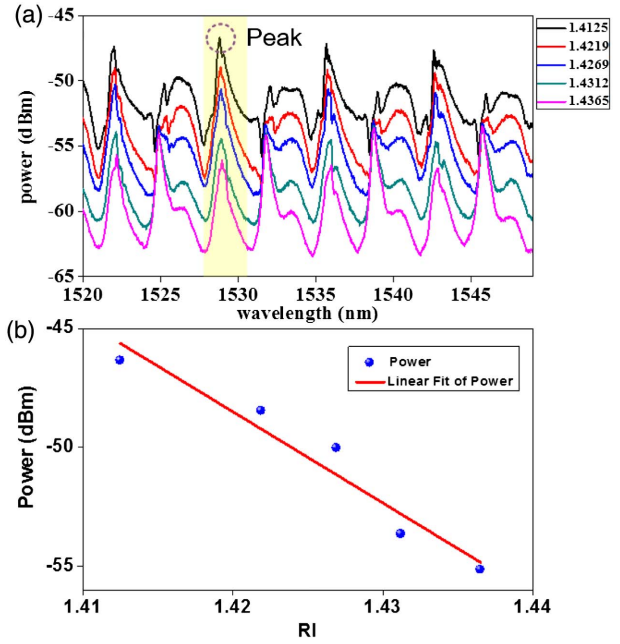

Fig. 8. (a) Spectra of the device in solutions with different refractive indices. (b) Intensity of the resonance peak at 1529 nm marked with a blue circle versus the refractive index.

The device can also be used as a refractive index sensor. We prepared several groups of solutions composed of ethanol and glycerine, with the refractive index varying from 1.4125 to 1.4365. The device was immersed into the solution and its reflection spectrum was taken and analyzed, noting that the microsphere coupling part should be away from the solution to avoid influencing the resonance condition. If there is no microsphere in the capillary, the spectrum will be a fairly flat line. Because of the great decrement of the reflection on the front end face of the capillary, the Fano resonances transformed into regular WGMs, as shown in Fig. 8(a). However, the peak wavelengths mainly stay at the same locations, which confirms that the microsphere coupling part is not touching the solution. As the refractive index increases, more light in the capillary wall will enter into the solution; as a result, the intensity of the resonance peaks decreases linearly, with a sensitivity of 431 dB/RIU observed around the peak at 1529 nm, as shown in Fig. 8(b).

4. CONCLUSION

In summary, we have investigated the characteristics of a cone-shaped inwall capillary-based microsphere resonator, and demonstrated its capability for temperature and refractive index sensing. The effects of various parameters on Fano resonances are studied in detail. It is found that, for the absolute value of slope, there exists a maximum point, which has great potential for optical switching and sensing with high performance. Moreover, we find the phenomenon of EIT when the phase difference δ is adopted as 0.5π, as long as the reflectivity r is close to 100%. Finally, we demonstrated the sensing characteristics of the structure by experiments, with a sensitivity of 10.9 pm/°C for temperature sensing based on the Fano resonance, while it was 431 dB/RIU for refractive index sensing based on the Lorentzian line shape.

Funding. National Natural Science Foundation of China (NSFC) (61377081, 61675126).

REFERENCES

1. A. B. Matsko and V. S. Ilchenko, "Optical resonators with whispering-gallery modes-part I: basics," IEEE J. Sel. Top. Quantum Electron. **12**, 3–14 (2006).
2. M. R. Foreman, J. D. Swaim, and F. Vollmer, "Whispering gallery mode sensors," Adv. Opt. Photon. **7**, 168–240 (2015).
3. F. Vanier, F. Côté, M. E. Amraoui, Y. Messaddeq, Y. A. Peter, and M. Rochette, "Low-threshold lasing at 1975 nm in thulium-doped tellurite glass microspheres," Opt. Lett. **40**, 5227–5230 (2015).
4. L. Xu, L. Liu, M. Li, X. Wu, and X. Tu, "Ultraviolet single-frequency coupled optofluidic ring resonator dye laser," Opt. Express **20**, 19996–20001 (2012).
5. P. Wang, M. Ding, G. S. Murugan, L. Bo, C. Guan, Y. Semenova, Q. Wu, G. Farrell, and G. Brambilla, "Packaged, high-Q, microsphere-resonator-based add-drop filter," Opt. Lett. **39**, 5208–5211 (2014).
6. L. Maleki, A. B. Matsko, A. A. Savchenkov, and V. S. Ilchenko, "Tunable delay line with interacting whispering-gallery-mode resonators," Opt. Lett. **29**, 626–628 (2004).
7. K. Luke, Y. Okawachi, M. R. E. Lamont, A. L. Gaeta, and M. Lipson, "Broadband mid-infrared frequency comb generation in a Si_3N_4 microresonator," Opt. Lett. **40**, 4823–4826 (2015).
8. S. Zhu, Y. Liu, L. Shi, X. Xu, S. Yuan, N. Liu, and X. Zhang, "Tunable polarization beam splitter based on optofluidic ring resonator," Opt. Express **24**, 17511–17521 (2016).

9. S. Fan, "Sharp asymmetric line shapes in side-coupled waveguide-cavity systems," Appl. Phys. Lett. **80**, 908–910 (2002).
10. R. Wang, M. Fraser, J. Li, X. Qiao, and A. Wang, "Integrated in-fiber coupler for microsphere whispering-gallery modes resonator excitation," Opt. Lett. **40**, 308–311 (2015).
11. B. Peng, Ö. Sahin Kaya, W. Chen, F. Nori, and L. Yang, "What is and what is not electromagnetically induced transparency in whispering-gallery microcavities," Nat. Commun. **5**, 5082 (2014).
12. C. Zheng, X. Jiang, S. Hua, L. Chang, G. Li, H. Fan, and M. Xiao, "Controllable optical analog to electromagnetically induced transparency in coupled high-Q microtoroid cavities," Opt. Express **20**, 18319–18325 (2012).
13. Y. F. Xiao, M. Li, Y. C. Liu, Y. Li, X. Sun, and Q. Gong, "Asymmetric Fano resonance analysis in indirectly coupled microresonators," Phys. Rev. A **82**, 13442–13444 (2010).
14. B. B. Li, Y. F. Xiao, C. L. Zou, and X. F. Jiang, "Experimental controlling of Fano resonance in indirectly coupled whispering-gallery microresonators," Appl. Phys. Lett. **100**, 021108 (2012).
15. Q. Li, T. Wang, Y. Su, M. Yan, and M. Qiu, "Coupled mode theory analysis of mode-splitting in coupled cavity system," Opt. Express **18**, 8367–8382 (2010).
16. Y. L. Shang, M. Y. Ye, and X. M. Lin, "Experimental observation of Fano-like resonance in a whispering-gallery-mode microresonator in aqueous environment," Photon. Res. **5**, 119–123 (2017).
17. Y. Zhou, D. Zhu, X. Yu, W. Ding, and F. Luan, "Fano resonances in metallic grating coupled whispering gallery mode resonator," Appl. Phys. Lett. **103**, 151108 (2013).
18. Y.-F. Xiao, L. He, J. Zhu, and L. Yang, "Electromagnetically induced transparency-like effect in a single polydimethylsiloxane-coated silica microtoroid," Appl. Phys. Lett. **94**, 231115 (2009).
19. X.-F. Jiang, C.-L. Zou, L. Wang, Q. Gong, and Y.-F. Xiao, "Whispering-gallery microcavities with unidirectional laser emission," Laser Photon. Rev. **10**, 40–61 (2016).
20. X. Zhang, Y. Yang, H. Shao, H. Bai, F. Pang, H. Xiao, and T. Wang, "Fano resonances in cone-shaped inwall capillary based microsphere resonator," Opt. Express **25**, 615–621 (2017).
21. Q. Deng, X. Li, Z. Zhou, and H. Yi, "Athermal scheme based on resonance splitting for silicon-on-insulator microring resonators," Photon. Res. **2**, 71–74 (2014).
22. X. Zhang, J. Xiong, F. Gu, J. Li, W. Wang, F. Pang, and T. Wang, "Fabrication and sensing characteristics of intrinsic Fabry–Perot interferometers in fiber tapers," Chin. Opt. Lett. **13**, 120602 (2015).